Journal of Petroleum Science and Engineering 200 (2021) 108195

Contents lists available at ScienceDirect

Journal of Petroleum Science and Engineering

journal homepage: http://www.elsevier.com/locate/petrol

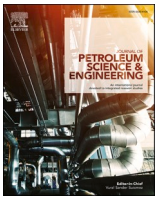

Mechanical characterization of Laffan and Nahr Umr anisotropic shales

Erhamah S. Alsuwaidi [a,*], Guifen Xi [b], Robert W. Zimmerman [a]

[a] Department of Earth Science and Engineering, Imperial College, London, UK
[b] ADNOC Offshore, Abu Dhabi National Oil Company, Abu Dhabi, United Arab Emirates

ARTICLE INFO

Keywords:
Shale
Anisotropy
Jaeger plane of weakness
Offshore Abu Dhabi

ABSTRACT

Geomechanics-related wellbore instability has become a major source of non-productive time in highly deviated wells drilled in oil and gas fields in offshore Abu Dhabi. These wells are drilled through two highly anisotropic shale formations, namely the Laffan shale formation and the Nahr Umr shale formation. Most of the models used in the oil and gas industry do not account for the strength and elastic anisotropy of shale. Therefore, a laboratory study was conducted to examine the strength and elastic anisotropy of shales using uniaxial compression tests and triaxial compression tests.

Jaeger's Plane of Weakness (JPW) model was used to understand the anisotropic failure behavior of highly laminated shales of the Laffan and Nahr Umr formations. This model assumes that for an anisotropic rock, there exists a plane of weakness that has strength properties (cohesion and angle of internal friction) different than the strength properties of the intact rock. By minimizing the Root Mean Square Error (RMSE), the experimental strength values of the samples, as measured at different orientations, were fitted to the JPW model.

Elastic moduli were also measured on these shales, as a function of orientation angle. The results showed that the moduli vary with angle according to the expected tensor transformation law. Therefore, the transverse isotropy assumption is a reasonable model to be used when dealing with these laminated sedimentary rocks.

1. Introduction

Understanding the mechanical behavior of anisotropic rocks is a subject of great importance in many engineering fields, such as civil and petroleum engineering. The anisotropic nature of rocks causes the mechanical properties to vary with direction, and ignoring these features can lead to errors when designing and solving engineering problems (Amadei, 1996). In sedimentary rocks, anisotropy originates from their laminated or stratified nature (Homand et al., 1993). The degree of rock anisotropy can be quantified by, for example, the ratio of the horizontal to vertical elastic modulus (Cho et al., 2012). Anisotropy also has a significant influence on the estimation of *in-situ* stress magnitude and direction, which in turn effects the process of well design (Gonano, 1984). Ignoring the anisotropic nature of laminated rocks when estimating the magnitude of the *in-situ* stresses can give results with errors of up to 25% (Hooker and Johnson, 1969).

The assumption of isotropy is a special case whereby a material is only defined by two independent elastic constants, and is considered fully symmetric (Lekhnitskii, 1981; Ting, 1996; Jaeger et al., 2007). On the other hand, an anisotropic material that has no plane of symmetry can be defined using as many as 21 independent elastic constants. In rock mechanics, there are several symmetry assumptions that can be used to decrease the number of independent elastic constants that define materials. Transverse isotropy is one symmetry model that can be used in rock mechanics to define an anisotropic material. A transversely isotropic material is defined using five independent elastic constants, and has one axis of rotational symmetry. Another type of symmetry is the orthotropic model. The orthotropic model assumes that there are three orthogonal planes of symmetry in a rock. This assumption reduces the number of elastic constants to nine (Cho et al., 2012). In the present study, a transversely isotropic model will be adopted, since this type of symmetry can best describe the lamination and foliation seen in sedimentary rocks (Song et al., 2004).

In order to estimate the strength properties of sedimentary rocks, a variety of failure criteria have been used to model the deformation behavior and estimate the strength properties. Mohr–Coulomb criterion is considered as one of most commonly used criterion in engineering applications. The Mohr–Coulomb model was developed in 1773, and states that failure in geological materials initiates along a plane when the shear stress along that plane reaches a critical value that can overcome the resistive frictional force plus a cohesive force (Jaeger et al., 2007). Al-Ajmi and Zimmerman (2005)

* Corresponding author.
E-mail address: e.alsuwaidi18@imperial.ac.uk (E.S. Alsuwaidi).

https://doi.org/10.1016/j.petrol.2020.108195
Received 1 May 2020; Received in revised form 20 October 2020; Accepted 28 November 2020
Available online 8 December 2020

investigated the Mohr–Coulomb criterion using data from the literature, and concluded that this criterion underestimates the cohesive strength of sedimentary rocks, because it neglects the effect of the intermediate principle stress in its formulation. Al-Ajmi and Zimmerman (2005) then investigated the Mogi–Coulomb failure criterion, which includes the effect of the intermediate principle stress, and showed that it can predict the strength of rocks more accurately than Mohr–Coulomb. The Mohr–Coulomb and Mogi–Coulomb criteria are applicable when a rock is assumed to be isotropic.

The anisotropic nature of laminated or stratified sedimentary rocks has an influence on their strength properties (Crawford et al., 2012). A great number of strength criteria claim to model the deformation behaviour of anisotropic rocks, to a certain degree of accuracy (Duveau et al., 1998). Pariseau (1968) explored Hill's theory of metal plasticity and modified it in order to develop a failure model for anisotropic rocks (Ambrose, 2014). His model showed that variation in rock strength was smooth and continuous when plotted against bedding-plane angle (Pariseau, 1968). Several researchers developed failure criteria based on the concept of the plane of weakness (Jaeger, 1960; Walsh and Brace, 1964; Hoek and Brown, 1981). The plane-of-weakness models were developed by observing the failure mechanism (Duveau et al., 1998). It was concluded that anisotropic rocks fail either through the rock matrix in shear, or by sliding along a plane of weakness, and that the failure stress is a function of the orientation of the applied load. Jaeger (1960) stated that, for a transversely isotropic rock, there is a plane of weakness on which the strength properties are less than the strength properties of the intact rock. Jaeger's (1960) plane-of-weakness (JPW) model also implies that the strength of a rock, when its bedding plane normal is parallel to the direction of the applied load, is equal to the strength of the rock when its bedding plane normal is perpendicular to the load.

Ambrose (2014) conducted triaxial stress experiments on two types of shale, and used the JPW and Pariseau models to evaluate the strength properties, concluding that both failure criteria predicted the strength of the rock reasonably well. The JPW model has an advantage over the Pariseau model, in that it uses the same strength properties that are typically used in industry (the cohesion and the angle of internal friction) to describe the failure along the plane of weakness (Ambrose et al., 2014). Ambrose (2014) also concluded that the prediction made by the JPW model concerning the strength of a rock when the bedding plane is normal or parallel to the load needs to be revisited. In the present study, the JPW model was used to evaluate the strength properties of two types of shale, extracted from offshore Abu Dhabi, in which transverse isotropy was assumed.

To evaluate the strength properties of an anisotropic material, at least three bedding-plane orientations are required (Barla, 1972). Prismatic or cylindrical specimens that have bedding-plane angles of 0°, 45° and 90° are sufficient for evaluating the strength of the rock matrix and the plane of weakness, and also to evaluate the five independent elastic properties (Barla, 1972; Worontnicki, 1994; Amadei, 1996). Previous researchers have used Saint-Venant's empirical equations to minimize the laboratory work and reduce the number of elastic constants from five to four. The shortcoming of this approach is that the assumptions used to develop Saint-Venant's empirical equations are different from the assumptions used to model transversely isotropic rocks, especially those rocks with high degrees of anisotropy (Worontnicki, 1994).

Togashi et al. (2017) modified the triaxial test cell by replacing the stationary top cap with a moving one in order to provide a smooth and frictionless boundary condition on the upper side of the specimen. This modification was intended to reduce the number of specimens needed to evaluate the five independent elastic constants to only one specimen. Moreover, this method helps with the identification of two directions of anisotropy for transversely isotropic sediments. The effectiveness of this approach has been confirmed theoretically, and is supported by a series of triaxial tests.

The mechanical and strength properties of shales in offshore Abu Dhabi were previously investigated using experimental procedures and using sonic measurements by several researchers. Yamamoto et al. (2002) conducted a direct shear test to evaluate the elastic properties of Nahr Umr shale. In the experiment, two samples with vertical and horizontal bedding plane orientations were used to measure the anisotropic elastic properties. The authors used the outcome of the experiment to calibrate geomechanical models for wells in offshore Abu Dhabi, and to determine the failure mode caused by the anisotropic nature of Nahr Umr shale. Grini et al. (2012) conducted a triaxial compression test on shale samples from offshore Abu Dhabi to quantify the degree of anisotropy in the strength properties. The experiment was conducted using samples with different bedding orientations to understand the difference between the failure through the intact rock and the failure along the plane of weakness. It was found that the strength was reduced to about 70% when the rock failed along the weak plane when compared to failure in the intact rock. Subbaih et al. (2018) evaluated the mechanical and strength properties of Laffan and Nahr Umr shale using sonic measure measurements and empirical equations. The purpose of their investigation was to understand the mechanical behavior associated with the failure of anisotropic rocks and its effect on drilling decisions.

Although several researchers have conducted experimental and empirical investigation on the elastic and strength behavior of Laffan and Nahr Umr shale, their analysis did not incorporate the failure criteria and elasticity models that take into account the anisotropic nature of shales seen in offshore Abu Dhabi.

The objective of this investigation is to conduct an extensive triaxial stress experiment to obtain strain measurements of samples with different bedding plane orientations. The results of the experiments will be used to model the elastic moduli with varying bedding plane orientation using the transversely isotropic model. Moreover, Mohr-Coulomb criterion and JPW model are used to evaluate the failure of the intact rock and the failure along the bedding plane of the shale samples, respectively. The outcome of this analysis will be used to calibrate geomechanical models in offshore Abu Dhabi to mitigate wellbore instability problems encountered there.

2. Theory and definitions

2.1. Constitutive models

The generalized Hooke's law is used to describe the constitutive relationship between strain and stress in linear, elastic, homogenous and continuous rock, and states that there is a linear relationship between the stress components and the strain components, with the relationship given by:

$$\varepsilon = S\sigma \tag{1}$$

where ε, S, and σ are the strain, the elastic compliance tensor, and the stress, respectively. The symmetry of the stress and strain components, and the existence of a strain energy function, can reduce the number of independent components of the elastic compliance tensor from 81 to 21. Lekhnitskii (1963) detailed the physical meaning of the compliance tensor, defining it by the following expression:

$$S = \begin{bmatrix} \frac{1}{E_x} & -\frac{\nu_{yx}}{E_y} & -\frac{\nu_{zx}}{E_z} & \frac{\eta_{x,yz}}{G_{yz}} & \frac{\eta_{x,xz}}{G_{xz}} & \frac{\eta_{x,xy}}{G_{xy}} \\ -\frac{\nu_{xy}}{E_x} & \frac{1}{E_y} & -\frac{\nu_{zy}}{E_z} & \frac{\eta_{y,yz}}{G_{yz}} & \frac{\eta_{y,xz}}{G_{xz}} & \frac{\eta_{y,xy}}{G_{xy}} \\ -\frac{\nu_{zx}}{E_x} & -\frac{\nu_{yz}}{E_y} & \frac{1}{E_z} & \frac{\eta_{z,yz}}{G_{yz}} & \frac{\eta_{z,xz}}{G_{xz}} & \frac{\eta_{z,xy}}{G_{xy}} \\ \frac{\eta_{yz,x}}{E_x} & \frac{\eta_{yz,y}}{E_y} & \frac{\eta_{yz,z}}{E_z} & \frac{1}{G_{yz}} & \frac{\mu_{yz,xz}}{G_{xz}} & \frac{\mu_{yz,xy}}{G_{xy}} \\ \frac{\eta_{xz,x}}{E_x} & \frac{\eta_{xz,y}}{E_y} & \frac{\eta_{xz,z}}{E_z} & \frac{\mu_{xz,yz}}{G_{yz}} & \frac{1}{G_{xz}} & \frac{\mu_{xz,xy}}{G_{xy}} \\ \frac{\eta_{xy,x}}{E_x} & \frac{\eta_{xy,y}}{E_y} & \frac{\eta_{xy,z}}{E_z} & \frac{\mu_{xy,yz}}{G_{yz}} & \frac{\mu_{xy,xz}}{G_{xz}} & \frac{1}{G_{xy}} \end{bmatrix} \tag{2}$$

where E, G and ν are the Young's modulus, shear modulus and Poisson's

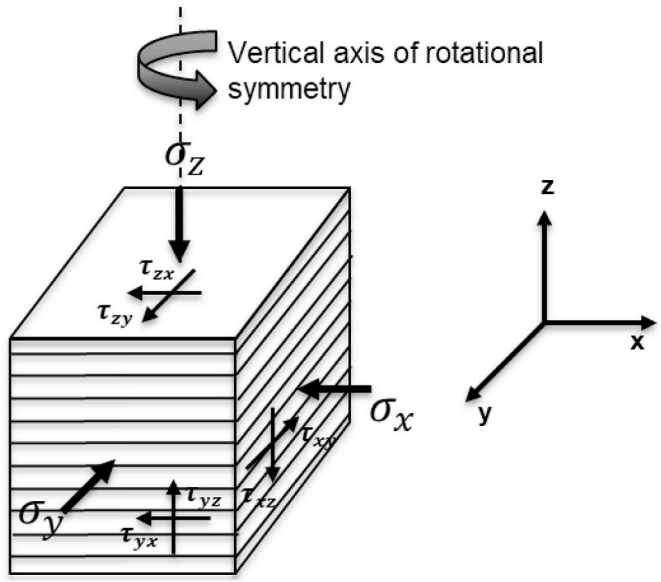

Fig. 1. Vertical transverse isotropy in layered rocks.

ratio, respectively; $\mu_{ij.kl}$ describes the shear on the plane "*ij*" that creates the tangential stress in the plane "*kl*"; $\eta_{k.ij}$ and $\eta_{ij.k}$ are the coefficients of mutual influence of the first type and the second type, respectively (Ong, 1994).

The kind of symmetry possessed by a material can simplify the expression of the elastic compliance tensor and reduce some of its components. A material can possess several kinds of symmetry, but the scope of this study embraced the symmetry possessed by shale. Shales have a kind of symmetry in which there is only one axis of elastic rotational symmetry (Amadei, 1983). This kind of symmetry is known as transverse isotropy. Fig. 1 illustrates an example of layered rocks that possess vertical transverse isotropy. If the axis of symmetry is normal to the *x*-*y* plane, the number of elastic constants is reduced from twenty-one to five:

$$E_x = E_y = E_h; \quad E_z = E_v \qquad (3)$$
$$\nu_{xy}=\nu_{yx}=\nu_h; \quad \nu_{zx}=\nu_{zy}=\nu_v$$
$$G_{yz} = G_{xz} = G_v; \quad G_{xy} = G_h = \frac{E_h}{2(1+\nu_h)}$$

where E_h and E_v are the horizontal Young's modulus and the vertical Young's modulus, respectively; ν_h and ν_v are the horizontal Poisson's ratio and the vertical Poisson's ratio, respectively; and G_h and G_v are the horizontal and vertical shear moduli, respectively (Dambley et al.,

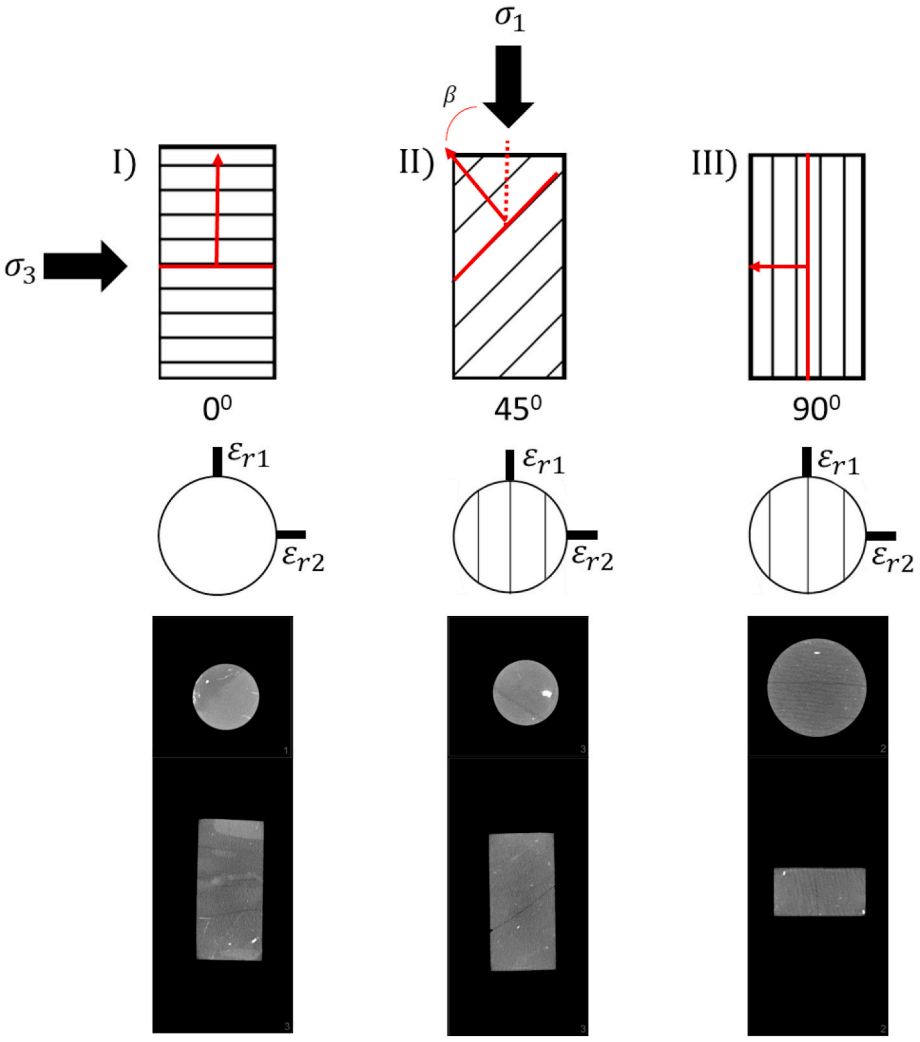

Fig. 2. Specimens for determining elastic properties.

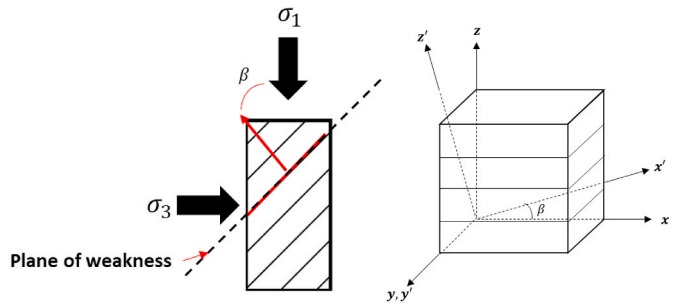

Fig. 3. Definition of angle β.

2019). Therefore, for a transversely isotropic medium, and using the simplified elastic compliance tensor, Hooke's law in the local coordinate system can be written as:

$$\begin{bmatrix}\varepsilon_x\\ \varepsilon_y\\ \varepsilon_z\\ \gamma_{yz}\\ \gamma_{zx}\\ \gamma_{xy}\end{bmatrix}=\begin{bmatrix}\frac{1}{E_h} & -\frac{\nu_h}{E_h} & -\frac{\nu_\nu}{E_\nu} & 0 & 0 & 0\\ -\frac{\nu_h}{E_h} & \frac{1}{E_h} & -\frac{\nu_v}{E_v} & 0 & 0 & 0\\ -\frac{\nu_\nu}{E_\nu} & -\frac{\nu_v}{E_v} & \frac{1}{E_v} & 0 & 0 & 0\\ 0 & 0 & 0 & \frac{1}{G_v} & 0 & 0\\ 0 & 0 & 0 & 0 & \frac{1}{G_v} & 0\\ 0 & 0 & 0 & 0 & 0 & \frac{1}{G_h}\end{bmatrix}\begin{bmatrix}\sigma_x\\ \sigma_y\\ \sigma_z\\ \tau_{yz}\\ \tau_{zx}\\ \tau_{xy}\end{bmatrix} \tag{4}$$

2.2. Determination of the elastic constants

The elastic properties of rocks that possess transverse isotropy can, in principle, be determined using only three specimens with three different bedding orientations (Barla, 1972; Amadei, 1996). Since only the horizontal and vertical elastic properties are needed to fully define the elastic nature of transversely isotropic rocks, specimens with bedding orientations of β = 0°, 45°, and 90° were tested in a uniaxial stress cell with strain gauges attached. Fig. 2 shows three specimens with different bedding-plane orientations undergoing uniaxial compression.

From Fig. 2, the following system of independent equations can be derived to evaluate the static elastic properties of a core.

Specimen I:

$$E_v=\frac{\sigma_a}{\varepsilon_a} \tag{5}$$

$$\nu_v=-\frac{\varepsilon_{ave_r}}{\varepsilon_a} \tag{6}$$

Specimen III:

$$E_h=\frac{\sigma_a}{\varepsilon_a} \tag{7}$$

$$\nu_h=-\frac{\varepsilon_{ave_r}}{\varepsilon_a} \tag{8}$$

where σ_a, ε_a, and ε_{ave_r} are the axial stress, axial strain, and the average radial strain, respectively.

For specimen II, Hooke's law must be transferred from the local coordinate system to the global coordinate system by a rotation β around the y-axis. The rotation between the local (x,y,z) coordinate system and the global (x',y',z') is presented in Fig. 3. To achieve this transformation, the compliance matrix will be rotated using the following tensorial transformation expression:

$$\boldsymbol{S}'=N\boldsymbol{S}N^T \tag{9}$$

where,

$$N=\begin{bmatrix} l_s^2 & m_s^2 & n_s^2 & 2m_sn_s & 2n_sl_s & 2l_sm_s\\ l_t^2 & m_t^2 & n_t^2 & 2m_tn_t & 2n_tl_t & 2l_tm_t\\ l_n^2 & m_n^2 & n_n^2 & 2m_nn_n & 2n_nl_n & 2l_nm_n\\ l_tl_n & m_tm_s & n_tn_n & m_tn_n+m_nn_t & n_tl_n+n_nl_t & l_tm_n+l_nm_s\\ l_nl_s & m_nm_s & n_nn_s & m_sn_n+m_nn_s & n_sl_n+n_nl_s & l_sm_n+l_nm_s\\ l_sl_t & m_sm_t & n_sn_t & m_sn_t+m_tn_s & n_sl_t+n_tl_s & l_sm_t+l_tm_s\end{bmatrix} \tag{10}$$

$$l_s=\cos\beta \quad m_s=0 \quad n_s=\sin\beta$$

$$l_t=0 \quad m_t=1 \quad n_t=0 \tag{11}$$

$$l_n=-\sin\beta \quad m_n=0 \quad n_n=\cos\beta$$

Hooke's law in global coordinates system is expressed as follows:

$$\begin{bmatrix}\varepsilon_x'\\ \varepsilon_y'\\ \varepsilon_z'\\ \gamma_{yz}'\\ \gamma_{zx}'\\ \gamma_{xy}'\end{bmatrix}=\begin{bmatrix}S_{11}' & S_{12}' & S_{13}' & 0 & S_{15}' & 0\\ S_{21}' & 22' & S_{23}' & 0 & S_{25}' & 0\\ S_{31}' & S_{32}' & S_{33}' & 0 & S_{35}' & 0\\ 0 & 0 & 0 & S_{44}' & 0 & 0\\ S_{51}' & S_{52}' & S_{53}' & 0 & S_{55}' & 0\\ 0 & 0 & 0 & 0 & 0 & S_{66}'\end{bmatrix}\begin{bmatrix}\sigma_x'\\ \sigma_y'\\ \sigma_z'\\ \tau_{yz}'\\ \tau_{zx}'\\ \tau_{xy}'\end{bmatrix} \tag{12}$$

This transformation will give the following expressions for the useful components of the compliance matrix in the global coordinate system:

$$S_{11}'=\frac{\sin^4\beta}{E_v}+\frac{\cos^4\beta}{E_h}+\frac{\sin^2 2\beta}{4}\left(-\frac{2\nu_v}{E_v}+\frac{1}{G_v}\right)$$

$$S_{12}'=\frac{\sin^2 2\beta}{4}\left(\frac{1}{E_h}+\frac{1}{E_v}-\frac{1}{G_v}\right)-\frac{\nu_v}{E_v}\left(\cos^4\beta+\sin^4\beta\right)$$

$$S_{13}'=-\sin^2\beta\left(\frac{\nu_h}{E_h}\right)-\cos^2\beta\left(\frac{\nu_v}{E_v}\right) \tag{13}$$

$$S_{33}'=\frac{\sin^4\beta}{E_h}+\frac{\cos^4\beta}{E_v}+\frac{\sin^2 2\beta}{4}\left(-\frac{2\nu_v}{E_v}+\frac{1}{G_v}\right)$$

The elastic properties of specimens I and III can also be calculated using the slope of the linear section of the stress-strain plot (Amadei, 1996). Specimen II was used to evaluate the shear modulus normal to the bedding-plane G_v using the S_{33}' equation.

3. Failure models

3.1. JPW model

Jaeger (1960) assumed that, for an isotropic rock that has a prescribed cohesion S_o and a coefficient of internal friction μ_o, there exists a weak plane that has different values for the cohesion S_w and the coefficient of internal friction μ_w. Using this idea, Jaeger (1960) was able to build a model capable of predicting failure when it occurs along the weak plane, known as the JPW model. JPW is one of the most commonly used criteria for failure of rocks that are transversely isotropic (Ambrose, 2014).

The linear Mohr criterion proposes that failure occurs along a plane when the shear stress τ on the plane is sufficient to overcome the internal friction force in addition to the cohesive force (Jaeger et al., 2007):

$$\tau=S_o+\sigma_n\mu_o \tag{14}$$

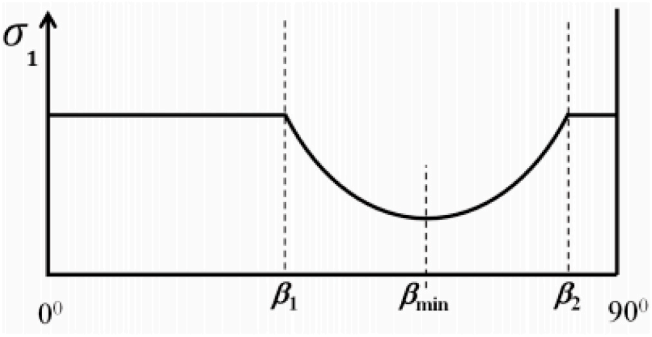

Fig. 4. JPW failure envelope (Ambrose, 2014).

$$\mu_o = \tan \varphi_o \tag{15}$$

where σ_n is the normal stress acting on the plane. Jaeger (1960) re-wrote the Mohr–Coulomb criterion by introducing the maximum shear stress τ_m that acts on any plane in the rock, and the mean normal stress at failure σ_m:

$$\tau = -\tau_m \sin 2\beta; \quad \sigma_n = \sigma_m - \tau_m \cos 2\beta \tag{16}$$

where β is the angle between the normal of the plane and the maximum principal stress, as shown in Fig. 3.

By substituting eqs. (16) and (15) into eq. (14), Jaeger (1960) was able to express the failure of intact isotropic rock, in terms of τ_m and σ_m:

$$\tau_m = \sigma_m \sin \varphi_o + S_o \cos \varphi_o \tag{17}$$

In Jaeger's (1960) investigation, he assumed that there was a plane within the rock that is weaker than the intact rock. This plane has a cohesion S_w and a coefficient of internal friction μ_w, and failure along this weak plane can be described, using the Mohr–Coulomb criterion, by:

$$\tau = S_w + \sigma_n \mu_w \tag{18}$$

$$\mu_w = \tan \varphi_w \tag{19}$$

The same substitution as the one utilized above can be used to express eq. (18), in terms of τ_m and σ_m, with further simplification:

$$\tau_m = \frac{\sigma_m \sin \varphi_w + S_w \cos \varphi_w}{\sin(2\beta - \varphi_w)} \tag{20}$$

The JPW model failure envelope can be drawn with respect to the maximum principal stress and the angle β. For intact rocks, the failure envelope will simply be a straight horizontal line, whereas, for failure along the weak plane, the failure envelope will resemble a semicircle, as shown in Fig. 4.

Fig. 5 shows the failure along the plane of weakness when analyzed using Mohr's circle. The arc between angles β_1 and β_2 represent the range in which failure will occur along the weak plane. It is useful to investigate the limits of the angle of the plane of weakness, β. This can be achieved by starting with eq. (18), and conducting some mathematical manipulations. The limits of angles β_1 and β_2 can be expressed as:

$$\beta_1 + \beta_2 = 90^o + \varphi_w \tag{21}$$

Looking at Fig. 4, β_{min} is located at the minimum strength of the failure envelope, and can be expressed as:

$$\beta_{min} = (\beta_1 + \beta_2)\frac{1}{2} = 45^o + \frac{\varphi_w}{2} \tag{22}$$

Ambrose (2014) showed that the JPW failure criterion can be expressed as the stress difference between the maximum (σ_1) and minimum (σ_3) principle stresses required to initiate failure as a function of the plane of weakness angle β:

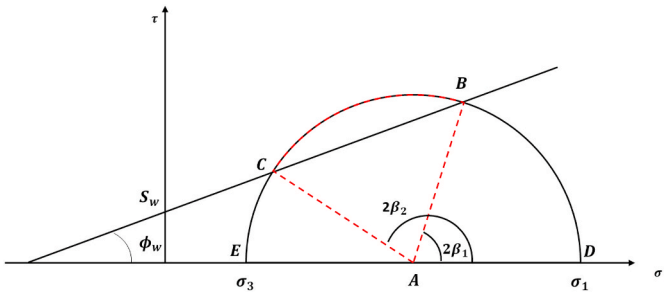

Fig. 5. JPW using Mohr diagram.

$$(\sigma_1 - \sigma_3) = \frac{2(S_w + \mu_w \sigma_3)}{[sin2\beta(1 - \mu_w \cot \beta)]} \tag{23}$$

From Eq. (23), if $\beta \to \frac{\pi}{2}$, the stress difference will approach infinity. This also happens to the stress difference if $\beta \to \varphi_w$. Therefore, to keep the right-hand side of eq. (23) positive and not infinite, a solution can only exist when $\varphi_w < \beta < \frac{\pi}{2}$ (Jaeger et al., 2007). To find the minimum magnitude of σ_1 needed to initiate slippage along the weak plane, eq. (20) must be differentiated to get:

$$\tan 2\beta_{min} = -\frac{1}{\tan \varphi_w} \tag{24}$$

and σ_{1min} is

$$\sigma_{1\min} = \sigma_3 + 2(S_w + \sigma_3 \tan \varphi_w) * \left[\sqrt{1 + \tan^2 \varphi_w} + \tan \varphi_w\right] \tag{25}$$

4. Experimental setup

The mechanical characterization of strength and elastic properties is essential for the calibration of log-derived mechanical properties. The outcome of the mechanical characterization of shale sections from offshore Abu Dhabi will be used to construct 1-D geomechanical models that will help with wellbore stability analyses for the area of interest (this will be the topic of a different paper). Rock mechanical testing took place in Abu Dhabi (UAE) in order to estimate the strength and elastic properties of two shale formations from offshore Abu Dhabi: the Laffan Shale and the Nahr Umr Shale. Four cores where extracted for the mechanical investigation, two from each formation.

As seen in Fig. 6, the Laffan and Nahr Umr formations consist of highly anisotropic transgressive shales, which are parts of the Aruma and Wasia groups, respectively. Laffan formation consists of Calcareous grey and brown shales, whereas Nahr Umr is considered varicolored from greenish grey to red to grey at the base. Both shale formations are characterized by fine lamination and high percentages of clay content.

Since shales are highly anisotropic, mechanical testing was conducted on cores with different bedding-plane orientations and using the JPW model, allowing the strength properties of the intact rock and the plane of weakness to be evaluated. To maintain quality control, the cores were wrapped in plastic film and sealed with wax. Moreover, the cores were plugged using inert mineral oil to minimize any chemical effects that might have arisen from using water based cutting fluids. Plugs were extracted from the cores and underwent (1) unconfined uniaxial compression testing, and (2) multi-stage triaxial compression testing.

The four shale samples were extracted from two different depths, as shown in Fig. 6. High resolution computed tomography imaging was used to investigate whether the cores contained any existing micro-fractures, to show the laminated characteristics of the shales, and to identify the failure mode of each plug, as shown in Fig. 7. The cores were plugged at different bedding orientations in order for the five elastic constants and the strength properties of the weak plane to be evaluated. A uniaxial compression test was conducted for the plugs with bedding-

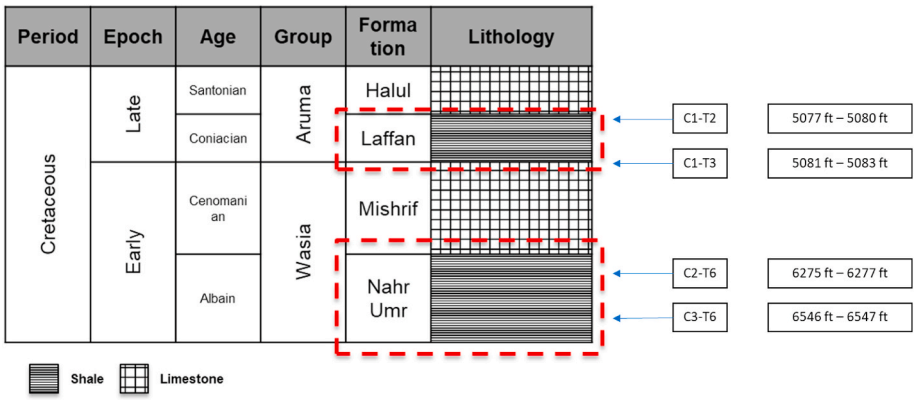

Fig. 6. Depths of the Laffan and Nahr Umr Formation core samples.

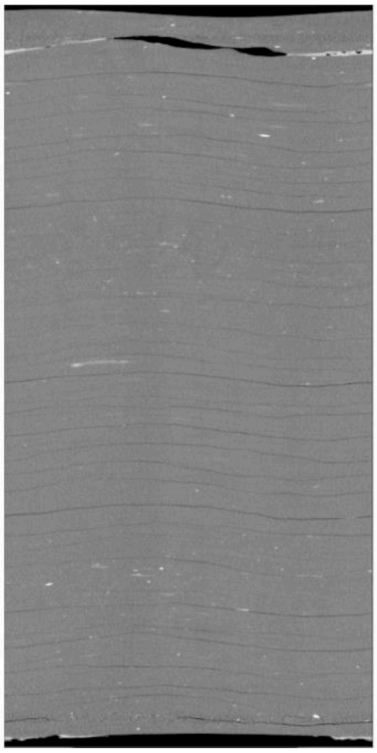

Fig. 7. CT scan of laminated core sample.

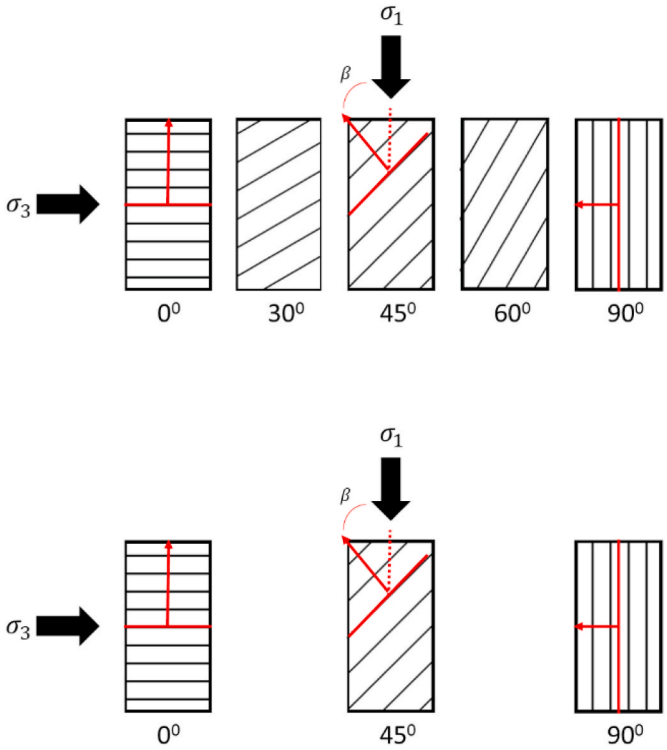

Fig. 8. Plan of bedding plane orientations. (a) testing plan for the uniaxial stress test; (b) testing plan for the triaxial stress test.

plane orientations of 0°, 30°, 45°, 60° and 90°. A triaxial compression test at two confinement levels was conducted for plugs with bedding-plane orientations of 0°, 45° and 90°. The outcomes of both experiments allowed the five independent elastic properties of transversely isotropic shale to be determined. The JPW model was then used to analyze strength variation with bedding-plane orientation, and to estimate the strength properties of the rock matrix and the plane of weakness. The outcomes of this study were then further used to conduct a geomechanical study for use in wellbore stability analysis (to be presented in a future paper).

For all the experiments, the plugs had nominal diameters of 1.0 inch or 0.75 inch, with lengths varying from 1.5 to 2 inches. The length to diameter ratio was kept equal or greater than two to minimize the plug-end effects on the outcomes of the tests (Mogi, 2006). For investigation of the strength anisotropy, the plugs had bedding-plane orientations of 0°, 30°, 45°, 60° and 90°. For the triaxial tests, only three bedding orientations were examined: 0°, 45° and 90° (Fig. 8). In the uniaxial stress test, a very small confinement pressure (Pc = 100 psi) is applied on the plugs to serve as lateral support.

Fig. 9 is a schematic diagram of the equipment used for the uniaxial and triaxial tests. In an unconfined compression test, a cylindrical plug is axially loaded to the point of failure. First, a confinement pressure is applied at a rate of 5 psi/s until it reaches the targeted confinement (Pc = 100 psi).

After letting the stress vessel stabilize, an axial load is applied by increasing the axial strain at a rate of 10^{-5}/s. The axial and radial strains are measured using cantilevered strain transducers. The measurements were recorded on a computer for elastic properties evaluation. The uniaxial compression strength of the plugs was defined as the maximum axial strength difference recorded using the test. The recorded axial and radial strain values were used to construct stress-strain curves. The elastic properties were estimated from the linear section of the stress-strain curves (Amadei, 1996). The strength and elastic properties were calculated for the plugs using the above-mentioned bedding orientations.

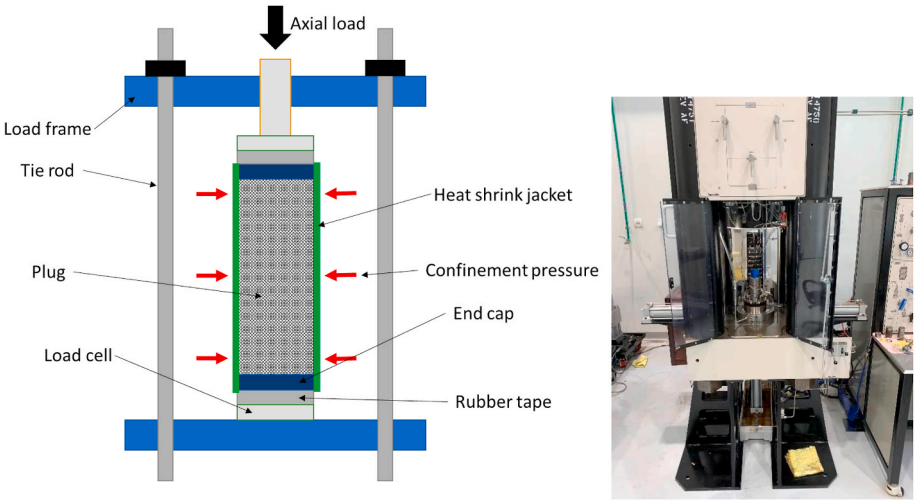

Fig. 9. Schematic diagram of the stress cell.

Table 1
Number of rock mechanical tests conducted on the four shale samples.

ID	Lithology	# Uniaxial tests	# Triaxial tests
C1T2	Laffan shale	4	6
C1T3	Laffan shale	5	6
C2T6	Nahr Umr shale	5	6
C3T6	Nahr Umr shale	5	6

Similarly to the uniaxial compression test, axial strain was applied to the core plug at the same rate as the uniaxial compression test rate until it reached failure. In a conventional triaxial compression test, confinement is constantly applied at different magnitudes ($\sigma_3 \geq 100$ psi). Before applying the axial load, the pressure vessel where the plug was installed was pressurized with confinement fluid at a rate of 5 psi/s until it reached the first targeted value, and then the vessel was left to stabilize. The confinement pressure was increased to higher values at a rate of 1 psi/s.

5. Results and discussion

To understand the mechanical behavior and anisotropic nature of the studied shales, uniaxial and triaxial stress tests were conducted on four samples, giving a total of forty mechanical tests. Table 1 shows the number of tests conducted in each experiment. Figs. 10–13 show the CT scans of the examined plugs before failure. The figures show the plugs arranged according to bedding plane orientations and confinement pressure. Figs. 14 and 15 show the stress-strain curves for the four shale samples at different confinement levels, for $\beta = 0°$, 45° and 90°. The peak strength of each plug was identified by the magnitude of the maximum differential stress shown on the stress-strain curves. The CT scans of the post-tests for the examined plugs can be seen in Figs. 16–19.

It can be observed from the curves in Figs. 14 and 15 that the peak strength of the four shale samples has a minimum at $\beta = 45°$ when compared to $\beta = 0°$ and 90°. The decrease in peak strength for angles around $\beta = 45°$ suggests failure along the weak plane. This can be also be seen in the CT scans in Figs. 16–19, were samples with $\beta = 30°$, 45°, and 60° failed along pre-existed plane of weakness. Moreover, it is expected, according to the JPW model, that these rocks will exhibit the same peak strengths at $\beta = 0°$ and $\beta = 90°$. In the present experiments, only one shale sample showed this feature: C2T6. The other shale samples show slightly higher peak strength for plugs that have $\beta = 90°$. This observation is consistent what was observed in the experiments performed by Cho et al. (2012) and Ambrose (2014).

To evaluate the cohesion and internal friction angle of the intact rock and the plane of weakness of the examined shale samples, the JPW model was implemented in MATLAB. The minimum root-mean-squared error (RMSE) was used to determine the set of strength properties that fit

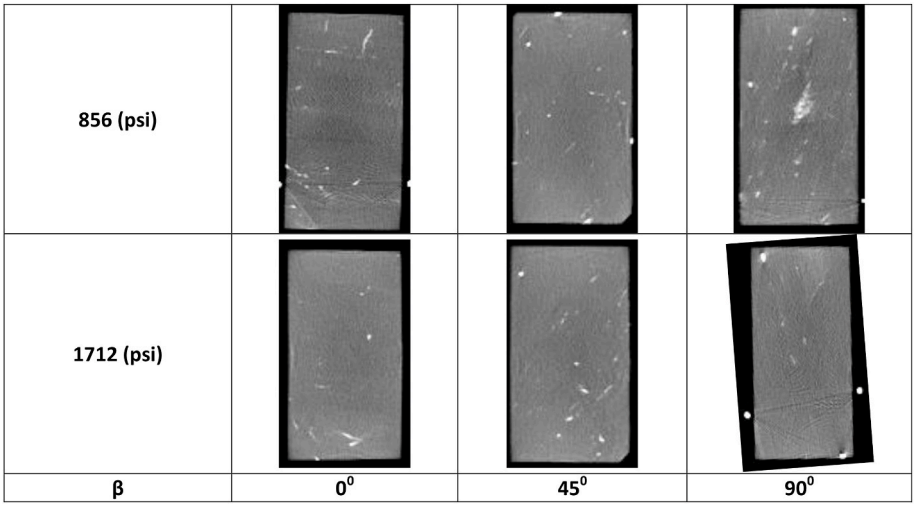

Fig. 10. CT scans of Laffan shale (C1T2) pre-test.

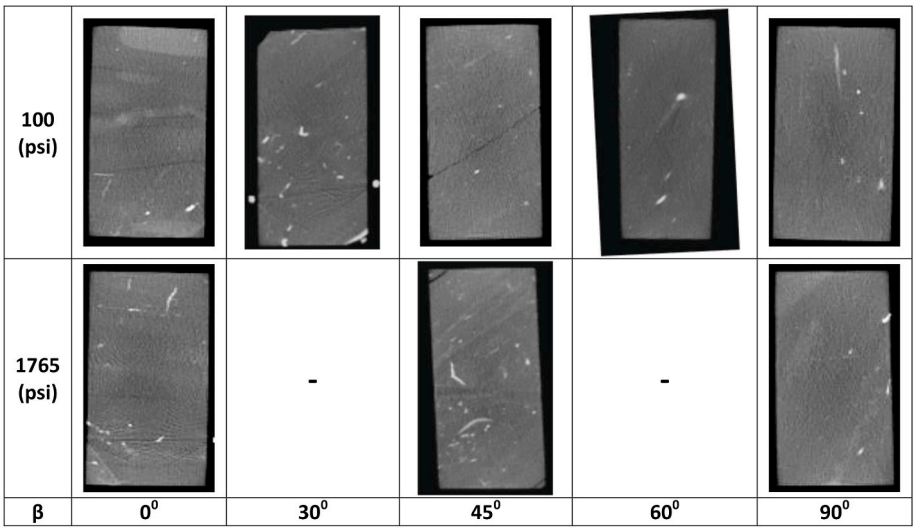

Fig. 11. CT scans of Laffan shale (C1T3) pre-test.

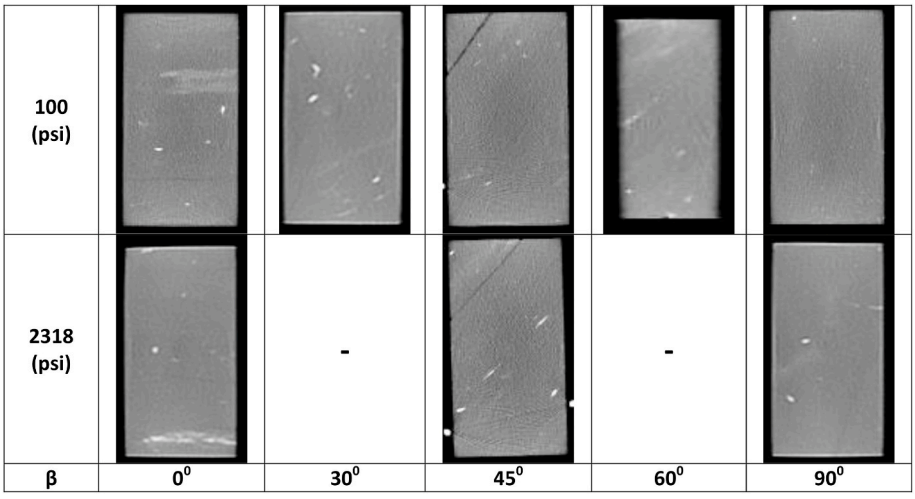

Fig. 12. CT scans of Nahr Umr shale (C2T6) pre-test.

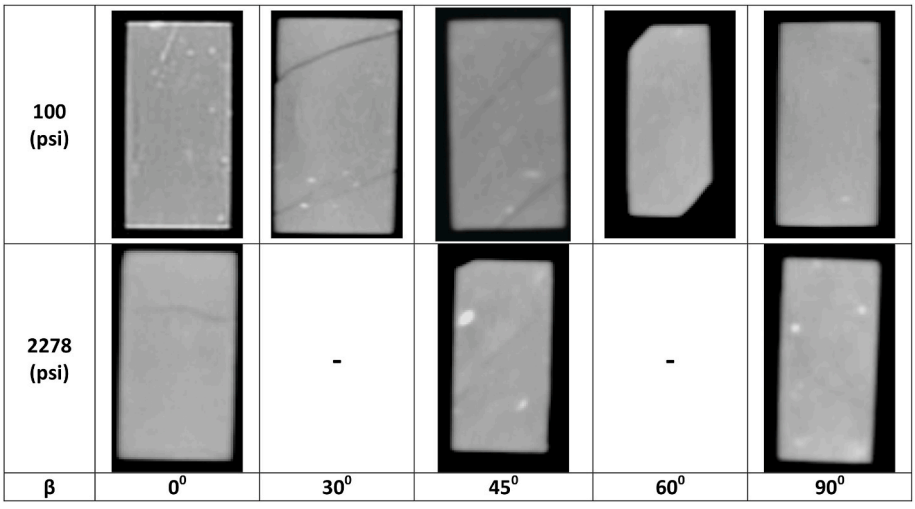

Fig. 13. CT scans of Nahr Umr shale (C3T6) pre-test.

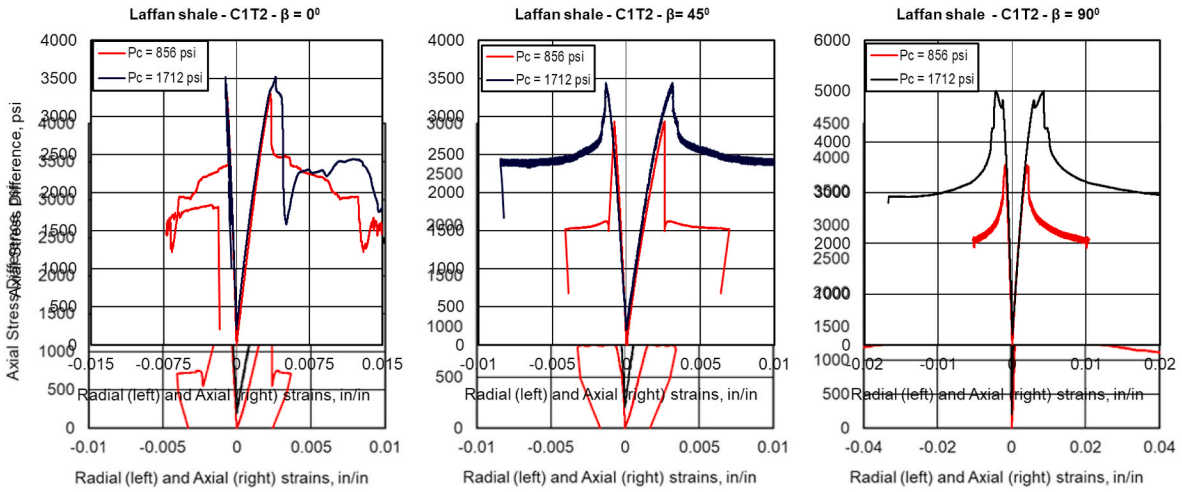

Fig. 14. Stress-strain curves at different confinement levels and different orientations for the four shale samples.

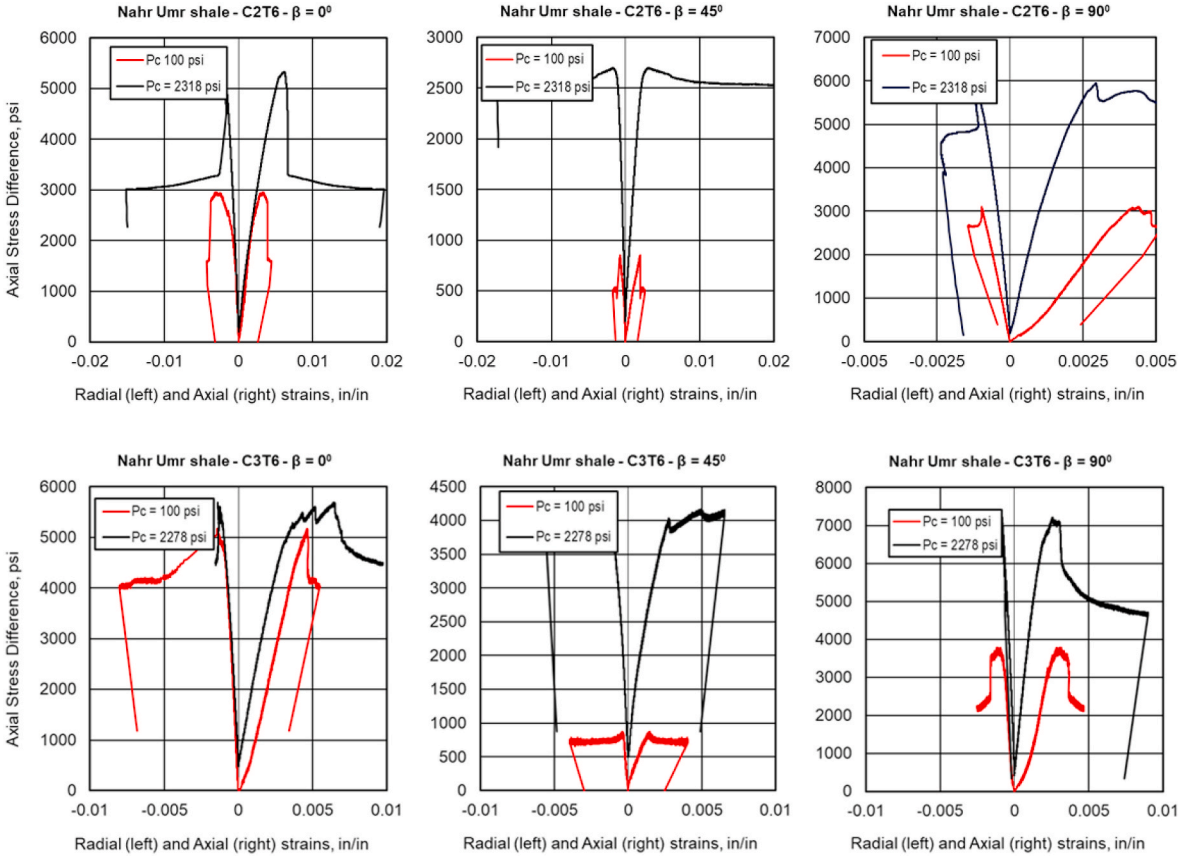

Fig. 15. Stress-strain curves at different confinement levels and different orientations for the four shale samples.

the experimental data:

$$RMSE = \sqrt{\frac{1}{N}\sum_{i=1}^{N}[\sigma_1(experimental) - \sigma_1(JPW)]^2} \quad (26)$$

Figs. 20 and 21 show the outcome of the curve-fitting procedure for the four shale samples. As mentioned above, it can be seen that there is a small increase in the strength of the shales between $\beta = 0^\circ$ and $\beta = 90^\circ$. For all samples, the minimum strength occurred at bedding-plane angles of between 50° and 60°. Also, it can be seen that for samples with $\beta =$ 30°, 45°, and 60°, failure took place along the bedding plane. This is consistent with the CT scans in Figs. 16–19. Looking at the results, there is some between-sample variability in terms of the strength properties. McGill and Raney (1970) investigated this variability and concluded that inhomogeneous rock samples tend to show such variation in strength properties. They used multiple-regression analysis to quantify this effect, finding that 25% of the variation in strength properties was related to the confinement pressure, 25% to the orientation and 10% to the applied strain rate. The remaining 40% was related to rock inhomogeneity and experimental error.

Table 2 shows the effective compressive strength (peak strength plus confinement pressure) obtained from the triaxial stress experiment for

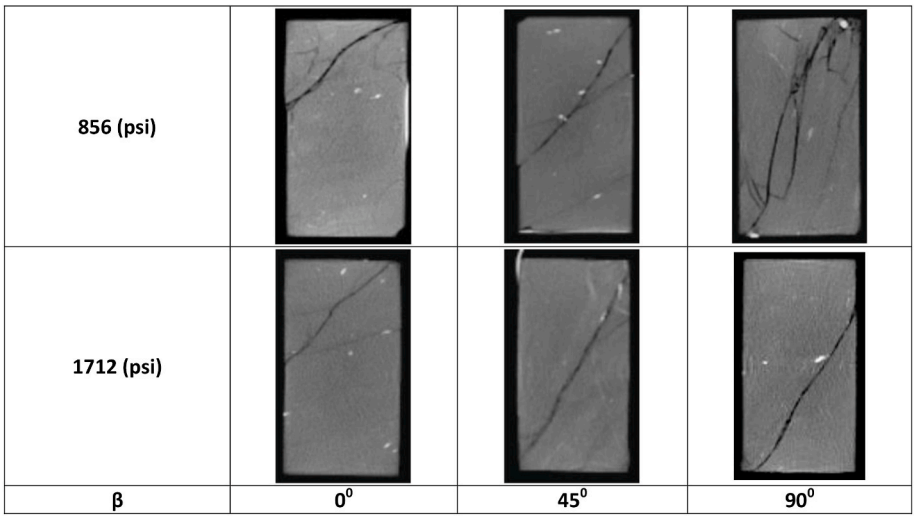

Fig. 16. CT scans of Laffan shale (C1T2) post-test.

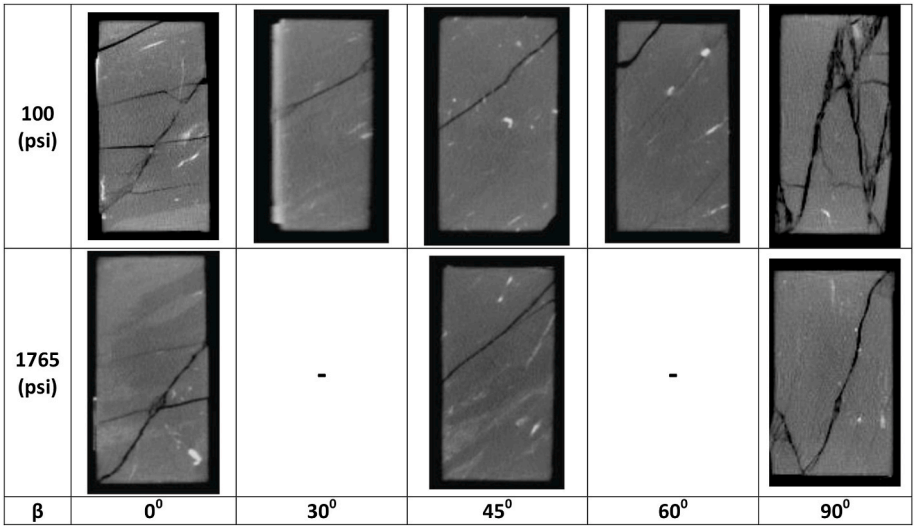

Fig. 17. CT scans of Laffan shale (C1T3) post-test.

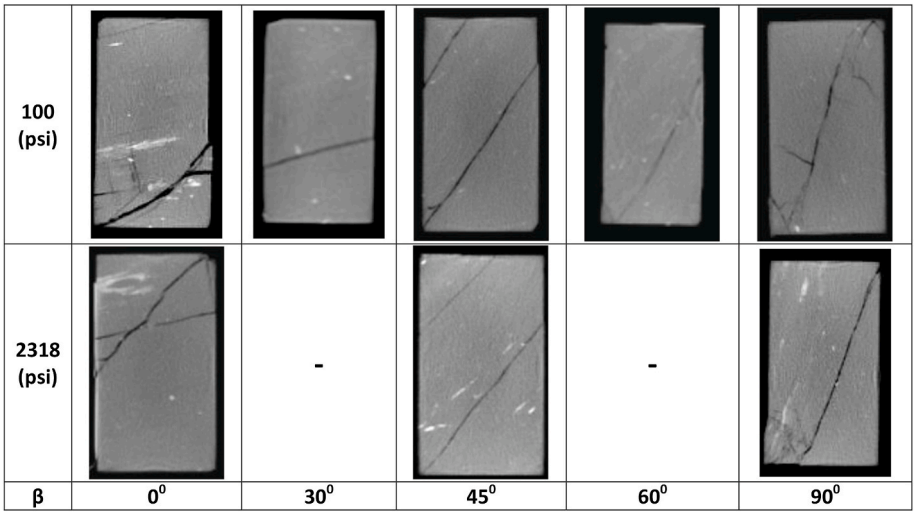

Fig. 18. CT scans of Nahr Umr shale (C2T6) post-test.

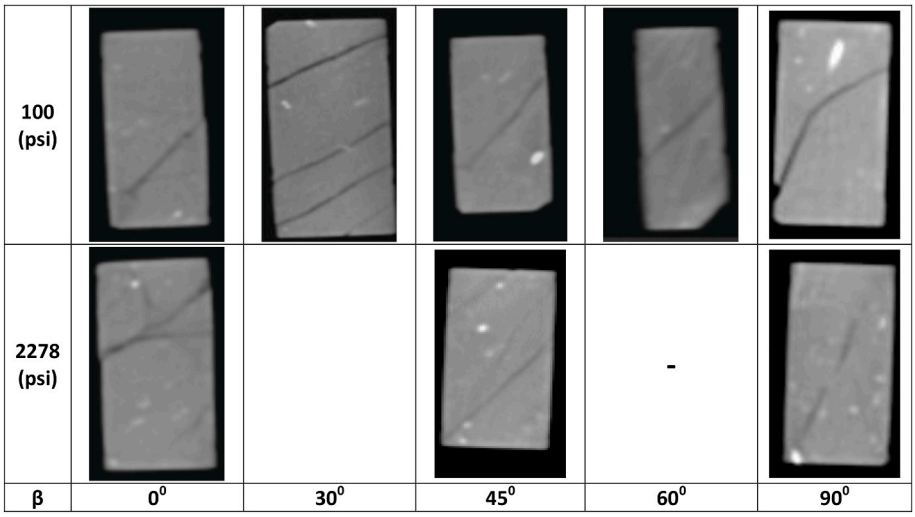

Fig. 19. CT scans of Nahr Umr shale (C3T6) post-test.

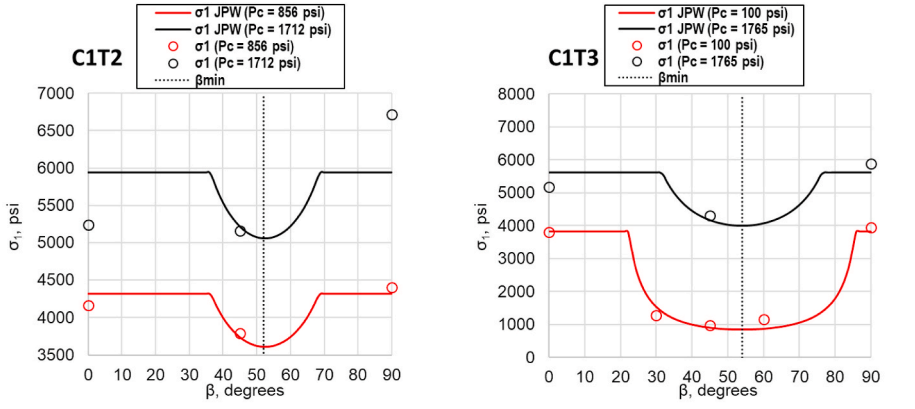

So (psi)	fo (degree)	Sw (psi)	fw (degree)	RMSE (psi)
980	18	825	15	434.5

So (psi)	fo (degree)	Sw (psi)	fw (degree)	RMSE (psi)
1800	2	240	18	233.3

Fig. 20. JPW model fit to experimental data points of Laffan shale samples.

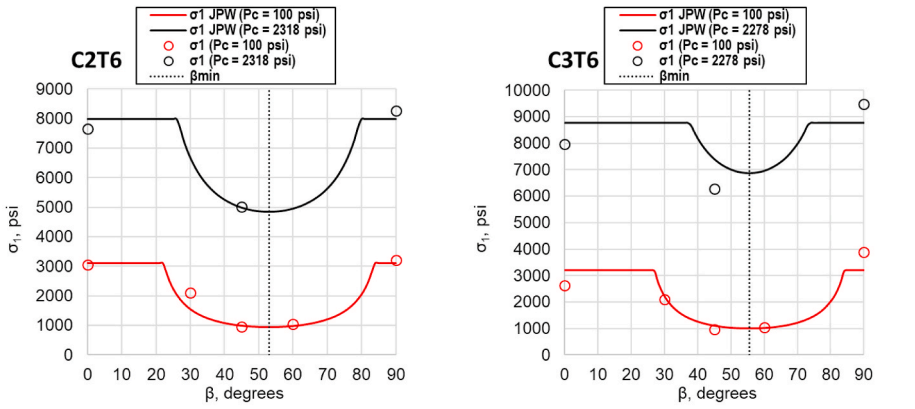

So (psi)	fo (degree)	Sw (psi)	fw (degree)	RMSE (psi)
973	22	348	16	210.1

So (psi)	fo (degree)	Sw (psi)	fw (degree)	RMSE (psi)
921	26	267	21	508.5152

Fig. 21. JPW model fit to experimental data points of Nahr Umr shale samples.

Table 2
Results of experiments.

Sample	β (degrees)	P_c (psi)	σ_1 (psi)	*SAR*	Average	
Laffan Shale (C1T2)	0	856	4164	1.20	1.19	1.57
	45	856	3791			
	90	856	4405			
Laffan Shale (C1T2)	0	1712	5236	1.17		
	45	1712	5157			
	90	1712	6714			
Laffan Shale (C1T3)	0	100	3808	2.60	1.95	
	30	100	1286			
	45	100	982			
	60	100	1155			
	90	100	3949			
Laffan Shale (C1T3)	0	1765	5178	1.30		
	45	1765	4314			
	90	1765	5877			
Nahr Umr Shale (C2T6)	0	100	3054	2.88	2.24	2.32
	30	100	2103			
	45	100	950			
	60	100	1043			
	90	100	3208			
Nahr Umr Shale (C2T6)	0	2318	7644	1.60		
	45	2318	5020			
	90	2318	8263			
Nahr Umr Shale (C3T6)	0	100	2630	3.24	2.40	
	30	100	2103			
	45	100	974			
	60	100	1043			
	90	100	3886			
Nahr Umr Shale (C3T6)	0	2278	7972	1.57		
	45	2278	6290			
	90	2278	9488			

the four shale samples. The strength anisotropic ratio (SAR) was used to quantify the degree of anisotropy in the shale samples. Ulusay (2014) defined SAR as the ratio of the average strength at $\beta = 0^\circ$ and $\beta = 90^\circ$, divided by the strength magnitude at $\beta_{min.}$ The SAR can be expressed in terms of the confining pressure and the strength properties as:

$$SAR = \left[\frac{\sigma_3(1+\sin\varphi_o)+2S_o\cos\varphi_o}{\sigma_3(1+\sin\varphi_w)+2S_w\cos\varphi_w}\right] * \frac{1-\sin\varphi_w}{1-\sin\varphi_o} \quad (27)$$

The SAR ratios for the Laffan Shale samples (C1T2 and C1T3) were 1.19 and 1.95, respectively, suggesting a degree of heterogeneity in this formation. The SAR value for the C1T3 shale sample was higher than for C1T2, which is consistent with the obvious difference in the magnitudes of the strength properties between the intact rock and the plane of weakness for both samples. For the Nahr Umr Shale, in terms of sample location, C2T6 had a degree of anisotropy that was a little less than the degree of anisotropy experienced by C3T6, at 2.24 and 2.40, respectively. From this investigation, it can be concluded that the Nahr Umr Shale has a greater strength anisotropy than does the Laffan Shale.

The strength of sedimentary rocks is an essential input for wellbore stability analysis. Assuming that shales will only fail through the intact rock in shear can result in borehole collapse, damaged drill strings, or even formation damage. Using the JPW model on the experimental results showed that there is a difference between the strength magnitudes of the intact rock and the plane of weakness. Implementing the effect of the plane of weakness in the calculation of the collapse pressure can result in a different pressure profile compared to the case of not including the effect. Lee et al. (2012) investigated the effect of including the bedding plane failure in the prediction of the minimum mud weight that is required to prevent borehole collapse. It was observed that the mud weight magnitude and the drilling direction were highly affected by the inclusion of strength anisotropy in the analysis.

The independent elastic constants can be evaluated from the linear sections of the stress-strain curves illustrated in Figs. 22 and 23. All samples initially showed a linear relationship between the stress and strain, until the curve transitioned to nonlinear behavior. Figs. 22 and 23 show the variation in the elastic constants, Young's modulus, and Poisson's ratio, with respect to the bedding-plane orientation. A general observation that can be derived from the figures is that all the samples showed similar trends in Young's modulus and Poisson's ratio when plotted against bedding-plane orientation. The Young's moduli (E_v) normal to the bedding plane were always less than the Young's moduli (E_h) parallel to the bedding plane. The magnitude of Young's modulus seems to be insensitive to the increase in confining pressure at a bedding-plane angle of 0°, whilst with increasing bedding-plane angle, this magnitude starts to respond to the increase in confinement pressure, showing a clear difference in magnitude among the three confinement pressures. Greater confining pressures correspond to higher Young's modulus magnitudes. For the Laffan Shale (C1T2), the vertical Young's modulus ranged from $E_v = 6.28$ GPa to $E_v = 7.30$ GPa, with a greater scatter observed at $\beta = 90^\circ$, ranging from $E_h = 9.95$ GPa to $E_h = 14.3$ GPa. Similar behavior was also noticed in the other shale samples (C1T3, C2T6, C3T6).

The Laffan Shale samples (C1T2 and C1T3) had anisotropic elasticity ratios (E_h/E_v) of 1.76 and 1.77, respectively, whilst the Nahr Umr Shale samples (C2T6 and C3T6) had ratios of 1.70 and 3.25, respectively. The large difference in the anisotropic elasticity ratios between C2T6 and C3T6 may be the result of the significant difference between the extraction depths, thus suggesting a degree of heterogeneity in the Nahr Umr Formation. The average anisotropic elasticity ratios for the Laffan and Nahr Umr Formations are 1.76 and 2.48, respectively, the Nahr Umr Formation having greater anisotropic elasticity than the Laffan Formation. Fig. 24 shows a comparison between the average values of the elastic constants for the four shale samples. The theoretical prediction of the Young's modulus was calculated using S_{33} in eq. (13), the solution is represented by the curve TH in Figs. 22 and 23. It can be seen that there is a reasonable match between the theoretical values of Young's modulus and the measured values from the experiments, suggesting that the type of anisotropy used (transverse isotropy) to model the results was good enough for the type of rocks studied in these experiments. Examining the relationship between the elastic anisotropy ratio and strength anisotropy ratio, it can be observed that there is a general trend between the two parameters. Nahr Umr shale showed higher degrees of anisotropy for both, the elastic modulus and the strength when compared to the ratios found for Laffan shale. This trend was also observed by Ambrose (2014), where he unsuccessfully attempted to find a direct relation between the strength parameters and the elastic constants. Sone and Zoback (2013) stated that the relation between the strength parameters and the elastic constants is not easy to explain quantitatively.

To carry out a comprehensive wellbore stability analysis, the stress distribution around the borehole plays a key role in drill design and decisions. A common practice in oil and gas petroleum is to consider isotropic elasticity when calculating the stress distribution. Setiawan and Zimmerman (2018) investigated the effect of implementing elastic anisotropy in stress distribution around the borehole. They used the Lekhnitskii-Amadei solution to perform this analysis. The results showed that higher stress concentrations were observed when applying anisotropic models, as compared to using isotropic models. Moreover, the difference between the isotropic and anisotropic elastic models can reach up to 25%.

6. Conclusions

This paper presented the results of rock mechanical experiments performed to characterize two shale formations in an offshore Abu Dhabi field in the Arabian Gulf area. Four shale samples were extracted from the Laffan Shale and Nahr Umr Shale Formations. Each formation was sampled at two different depths. The cylindrical plugs with different bedding-plane orientations were subjected to uniaxial and triaxial compression tests. Testing the plugs in different bedding-plane orientations was necessary in order to be able to evaluate the JPW model and

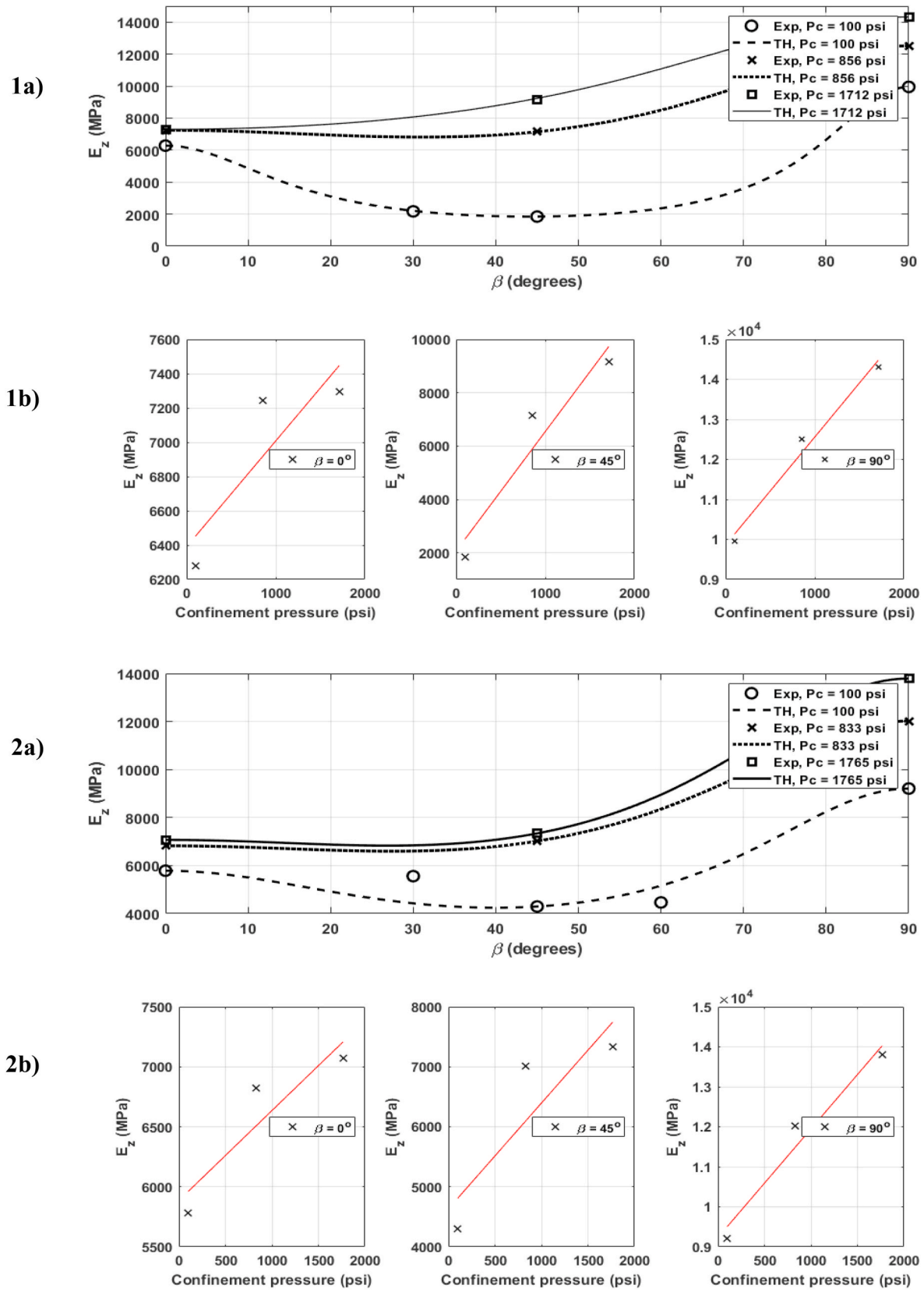

Fig. 22. (1a) and (2a) show the apparent Young's moduli variation with bedding plane angle, at increasing confinement levels for Laffan samples (C1T2) and (C1T3), respectively. (1b) and (2b) show the sensitivity of the apparent Young's modulus to changes in confinement levels for different bedding orientations, for Laffan samples (C1T2) and (C1T3), respectively.

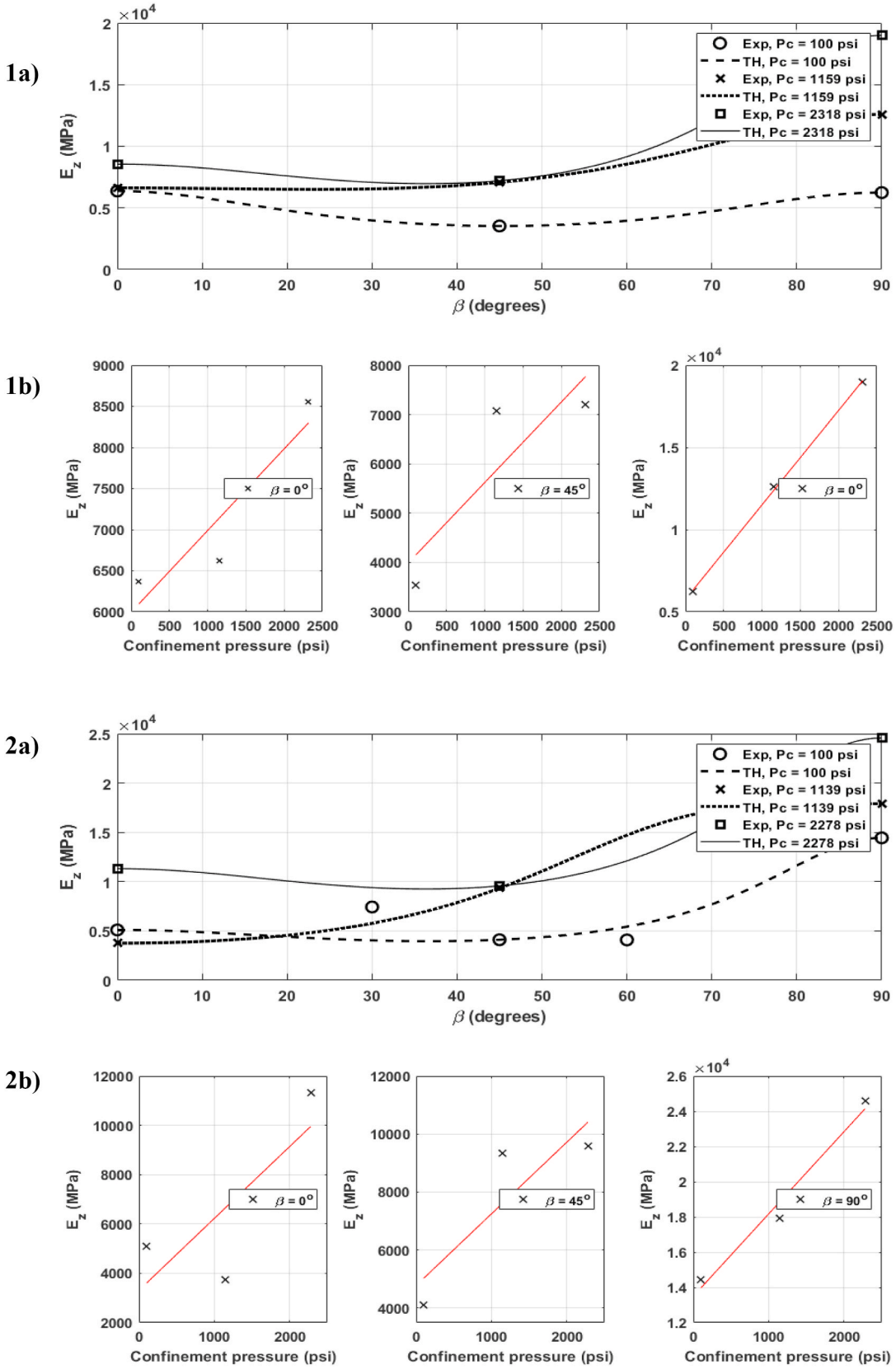

Fig. 23. (1a) and (2a) show the apparent Young's moduli variation with bedding plane angle, at increasing confinement levels for Nahr Umr samples (C1T2) and (C1T3), respectively. (1b) and (2b) show the sensitivity of the apparent Young's modulus to changes in confinement levels for different bedding orientations, for Nahr Umr samples (C1T2) and (C1T3), respectively.

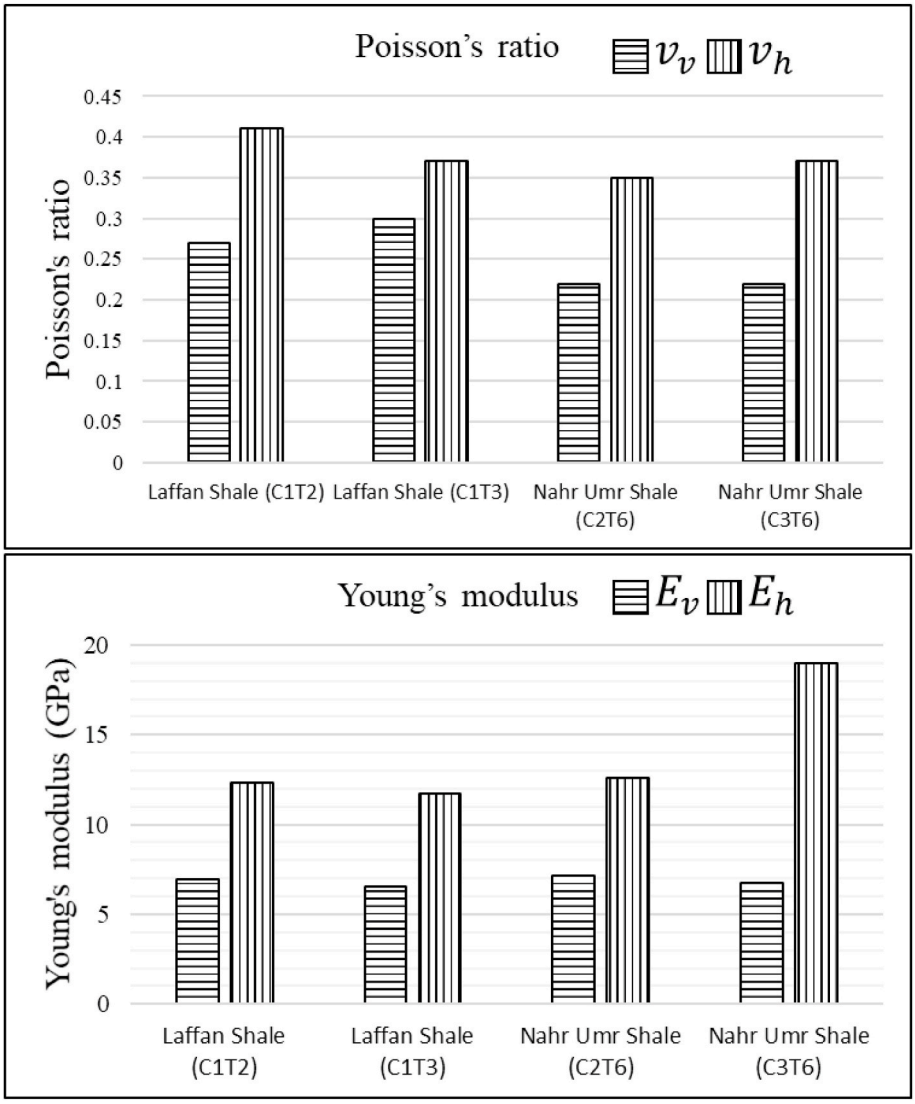

Fig. 24. A visual comparison between the average values of the elastic constants for the four shale samples.

to investigate the sensitivity of the elastic constants to changes in bedding-plane angle.

The JPW modeling of the Laffan Shale samples indicated that this formation is inhomogeneous because different strength properties for the weak plane were determined from the two samples. The lower part of the Laffan Shale seemed to be more anisotropic than the upper part. The Nahr Umr Shale had a lower degree of heterogeneity in terms of strength properties than did the Laffan Shale. The degree of anisotropy in the two Nahr Umr Shale samples was relatively similar, even though the two samples were extracted some distance apart. Moreover, the average values of the strength anisotropy ratio for the two samples suggest that Nahr Umr Shale is more anisotropic than the Laffan Shale (anisotropy values of 2.32 and 1.57, respectively).

The behavior of the independent elastic constants with respect to the bedding planes was investigated using the results of the strain measurements from the uniaxial and triaxial stress experiments. The elastic constants, Young's modulus and Poisson's ratio, had maximum values when the bedding plane normal was perpendicular to the direction of the applied stress. Also, the results showed that the sensitivity of Young's modulus to the change in confinement pressure became more significant at higher bedding-plane angles. Moreover, the theoretical variation of Young's modulus with orientation angle gave a reasonable match with the measured values, suggesting that transverse isotropy is a good assumption to be used when modeling the Laffan and Nahr Umr Shale Formations.

Declaration of competing interest

The authors declare that they have no known competing financial interests or personal relationships that could have appeared to influence the work reported in this paper.

Acknowledgements

This study was fully funded by Abu Dhabi National Oil Company.

Appendix A. Supplementary data

Supplementary data to this article can be found online at https://doi.org/10.1016/j.petrol.2020.108195.

Credit author statement

Erhamah S. Alsuwaidi: Methodology, Software, Investigation, Writing – original draft, Visualization. Robert W. Zimmerman: Validation, Writing – review & editing, Supervision. Guifen Xi: Resources,

Writing – review & editing

References

Al-Ajmi, A., Zimmerman, R.W., 2005. Relation between the Mogi and the coulomb failure criteria. Int. J. Rock Mech. Min. Sci. 42 (3), 431–439.

Amadei, B., 1983. Rock Anisotropy and the Theory of Stress Measurements. Springer-Verlag, Berlin.

Amadei, B., 1996. Importance of anisotropy when estimating and measuring in situ stresses in rock. Int. J. Rock Mech. Min. Sci. Geomech. Abstr. 33 (3), 293–325.

Ambrose, J., 2014. Failure of Anisotropic Shales under Triaxial Stress Conditions. PhD thesis. Imperial College London.

Ambrose, J., Zimmerman, R., Suarez-Rivera, R., 2014. Failure of shales under triaxial compressive stress. In: 48th US Rock Mechanics and Geomechanics Symposium, Paper ARMA 2014–7506.

Barla, G., 1972. In: Müller, L. (Ed.), Rock Anisotropy - Theory and Laboratory Testing, Rock Mechanics. Springer, Vienna, pp. 131–169.

Cho, J.-W., et al., 2012. Deformation and strength anisotropy of Asan gneiss, Boryeong shale, and Yeoncheon schist. Int. J. Rock Mech. Min. Sci. 50, 158–169.

Crawford, B.R., DeDontney, N.L., Alramahi, B.E., Ottesen, S., 2012. Shear strength anisotropy in fine-grained rocks. In: Proceedings of the 46th U.S. Rock Mechanics Symposium, Paper ARMA 2012-290.

Dambly, M.L.T., Nejati, M., Vogler, D., Saar, M.O., 2019. On the direct measurement of shear moduli in transversely isotropic rocks using the uniaxial compression test. Int. J. Rock Mech. Min. Sci. 113, 220–240.

Duveau, G., Shao, J.F., Henry, J.P., 1998. Assessment of some failure criteria for strongly anisotropic geomaterials. Mech. Cohesive-Frict. Mater. 3 (1), 1–26.

Gonano, L.P., 1984. Critical evaluation of rock behaviour for in-situ stress determination using overcoring methods. Int. J. Rock Mech. Min. Sci. 21 (3), A98.

Grini, M., et al., 2012. Extended reach drilling optimization in layer A shale through geomechanical characterization. In: Abu Dhabi International Petroleum Conference and Exhibition, Paper SPE 162491-MS.

Hoek, E., Brown, E.T., 1981. Empirical strength criterion for rock masses. Journal of the Geotechnical Engineering Division ASCE 106 (9), 1013–1035, 1980.

Homand, F., Morel, E., Henry, J.-P., Cuxac, P., Hammade, E., 1993. Characterization of the moduli of elasticity of an anisotropic rock using dynamic and static methods. Int. J. Rock Mech. Min. Sci. Geomech. Abstr. 30 (5), 527–535.

Hooker, V.E., Johnson, C.F., 1969. Near-surface Horizontal Stresses Including the Effects of Rock Anisotropy. U.S. Dept. of the Interior, Bureau of Mines, Washington, DC.

Jaeger, J.C., 1960. Shear failure of anistropic rocks. Geol. Mag. 97 (1), 65–72.

Jaeger, J.C., Cook, N.G.W., Zimmerman, R.W., 2007. Fundamentals of Rock Mechanics, fourth ed. John Wiley & Sons, Hoboken.

Lee, H., et al., 2012. A wellbore stability model for formations with anisotropic rock strengths. J. Petrol. Sci. Eng. 96 (97), 109–119.

Lekhnitskii, S.G., 1963. Theory of Elasticity of an Anisotropic Elastic Body. Holden-Day, San Francisco.

Lekhnitskii, S.G., 1981. Theory of Elasticity of an Anisotropic Body. Mir, Moscow.

McGill, G.E., Raney, J., 1970. Experimental study of faulting in an anisotropic, inhomogeneous dolomitic limestone. GSA Bulletin 81 (10), 2949–2958.

Mogi, K., 2006. Experimental Rock Mechanics. Taylor & Francis, London.

Ong, S., 1994. Borehole Stability. University of Oklahoma. PhD thesis.

Pariseau, W.G., 1968. Plasticity theory for anisotropic rocks and soil. In: Proceedings of the 10th U.S. Symposium on Rock Mechanics, Austin, Texas, p. 30.

Setiawan, N.B., Zimmerman, R.W., 2018. Wellbore breakout prediction in transversely isotropic rocks using true-triaxial failure criteria. Int. J. Rock Mech. Min. Sci. 112, 313–322.

Sone, H., Zoback, M.D., 2013. Mechanical properties of shale-gas reservoir rocks. Part 2: ductile creep, brittle strength, and their relation to the elastic modulus. Geophysics 78 (5), D393–D402.

Song, I., Suh, M., Woo, Y.-K., Hao, T., 2004. Determination of the elastic modulus set of foliated rocks from ultrasonic velocity measurements. Eng. Geol. 72 (3), 293–308.

Subbaih, S.K., et al., 2018. Chemo-mechanical behavior for UAE shales and mud design for wellbore stability. In: Abu Dhabi International Petroleum Conference and Exhibition, Paper SPE 192905-MS.

Ting, T.C.T., 1996. Anisotropic Elasticity Theory and Applications. Oxford University Press, New York.

Togashi, Y., Kikumoto, M., Tani, K., 2017. An experimental method to determine the elastic properties of transversely isotropic rocks by a single triaxial test. Rock Mech. Rock Eng. 50, 1–15.

Ulusay, R., 2014. The ISRM Suggested Methods for Rock Characterization, Testing and Monitoring. Springer, Dordrecht.

Walsh, J.B., Brace, W.F., 1964. A fracture criterion for brittle anisotropic rock. J. Geophys. Res. 69 (16), 3449–3456.

Worontnicki, G., 1993. CSIRO triaxial stress measurement cell. In: Rock Testing and Characterization. Elsevier, Oxford, pp. 329–394.

Yamamoto, K., et al., 2002. A mechanical model of shale instability problems offshore Abu Dhabi. In: Abu Dhabi International Petroleum Conference and Exhibition, Paper SPE 78494-MS.